Catalysis Science & Technology

PAPER

Cite this: *Catal. Sci. Technol.*, 2019, **9**, 4374

Mechanistic role of water in HSSZ-13 catalyzed methanol-to-olefins conversion†

Praveen Bollini, [a] Thomas T. Chen, [b] Matthew Neurock*[b] and Aditya Bhan *[b]

Co-feeding water leads to a simultaneous attenuation of chain initiation and chain termination rates in HSSZ-13 catalyzed methanol-to-olefins (MTO) conversion. Density functional theory calculations and transient stoichiometric experiments support the plausibility of formaldehyde hydrolysis occurring over zeolitic Brønsted acid sites at MTO-relevant temperatures. A monotonic decrease in MTO chain initiation and termination rates, and a concurrent monotonic increase in total turnovers as a function of water co-feed partial pressure are consistent with the occurrence and mechanistic relevance of formaldehyde hydrolysis effected by co-fed water. Initiation/termination rates and total turnovers normalized by their corresponding values in the absence of water co-feeds at the same temperature show the expected trends as a function of reaction temperature, assuming equilibrium between formaldehyde and methanediol. These results underscore the implications of formaldehyde hydrolysis chemistry when assessing the mechanistic role of water in methanol-to-olefins conversion specifically, and deactivation mechanisms in zeolite-catalyzed hydrocarbon conversion processes more generally.

Received 24th May 2019,
Accepted 14th July 2019

DOI: 10.1039/c9cy01015g

rsc.li/catalysis

1. Introduction

Methanol-to-olefins (MTO) conversion—the final processing step in converting gasifiable carbon-based feedstock to light-olefins (ethene and propene)[1]—is an autocatalytic process,[2,3] the propagation steps of which can be compendiously depicted using a dual-cycle hydrocarbon pool schematic comprised of olefinic and aromatic methylation/cracking events.[4–10] This dual-cycle scheme describes the interconversion between hydrocarbon chain carriers and their role in ethene and propene formation, but does not delineate the mechanism of transformation of active chain carriers to inactive ones. Recent reports correlating improvements in catalyst lifetime with lower average local methanol pressures,[11] operation in a continuous stirred tank reactor (CSTR) configuration instead of a plug flow reactor configuration (PFR),[12] or using dimethyl ether as feed instead of methanol[13–15] helped identify local methanol pressure as a key factor affecting catalyst lifetime. Shorter catalyst lifetimes resulting from co-feeding formaldehyde with methanol over HSSZ-13[11] and HZSM-5[14,16] point to the critical role formaldehyde plays in catalyst deactivation. The higher hydrogen transfer product yields (5×) for methanol-containing feeds compared to pure olefin feeds, and the greater sensitivity of hydrogen transfer product yields to contact time below 100% methanol conversion than above[17,18] also implicate formaldehyde, formed by the transfer dehydrogenation of methanol, as an accelerant for catalyst deactivation. Higher relative rates of hydrogen transfer to methylation in methanol–isobutene reactions compared to dimethyl ether-isobutene reactions over HZSM-5 at 673 K provide further evidence of the role of methanol as a hydride donor.[15] Recent reports correlating increasing proximity between formaldehyde-scavenging Y_2O_3 domains and HSAPO-34 with a decrease in chain initiation rates,[19] a 5.5-fold increase in aromatics selectivity observed on co-feeding 3 carbon% formaldehyde with propylene over HZSM-5 at 623 K,[20] as well as a 5-fold increase in aromatics selectivity on cofeeding 5 carbon% formaldehyde with methanol over HZSM-5 at 748 K[16] suggest that formaldehyde plays a critical role in accelerating not only chain termination steps leading to catalyst deactivation but also chain initiation steps responsible for the buildup of the hydrocarbon pool. Lercher and coworkers have further investigated the chemistry responsible for formaldehyde-mediated chain initiation,[16] in part by cofeeding 2 carbon% $H^{13}CHO$ with unlabeled methanol and 1-butene over HZSM-5 at 748 K, in which significantly higher ^{13}C fractions were measured in C_4–C_5 dienes and aromatics compared to C_2–C_5 olefins and C_1–C_4 paraffins. The authors attributed these higher ^{13}C fractions to Prins reaction of 1-butene with formaldehyde followed by dehydration to form pentadiene and water. These data are consistent with earlier

[a] *Department of Chemical & Biomolecular Engineering, University of Houston, 4722 Calhoun Rd., Houston, TX 77004, USA*
[b] *Department of Chemical Engineering and Materials Science, University of Minnesota, Twin Cities, 421 Washington Avenue SE, Minneapolis, MN 55455, USA. E-mail: abhan@umn.edu, mneurock@umn.edu*

† Electronic supplementary information (ESI) available. See DOI: 10.1039/c9cy01015g

proposals by Langner suggesting that formaldehyde formed in the transfer dehydrogenation of methanol undergoes Prins condensation reactions with olefins to form what are now understood to be hydrocarbon chain carriers.[21]

Water co-feeds have been shown to increase the time for which the catalyst effects 100% methanol conversion over HSAPO-34,[22,23] mordenite,[24] and HZSM-58,[25] as well as decrease the carbon deposited per gram catalyst at equivalent times-on-stream over HSAPO-34 at 673 K,[26,27] HSAPO-18 at 623 K,[28] and HZSM-5 at 623 K.[29] Specifically, Wu and Anthony reported that an optimal water-to-methanol ratio of 4 leads to an 8-fold increase in HSAPO-34 catalyst lifetime at 673 K (as represented by the time required for methanol conversion to drop below 100%) relative to the case of a pure methanol feed.[23] Marchi and Froment reported HSAPO-34 cumulative C_2–C_4 olefin yields that increased monotonically from 28 to 38 g_{olefin} $(g_{MeOH})^{-1}$ when the weight fraction of water in the water–methanol feed was increased from 0 to 10 weight%.[22] Ghavipour *et al.* found that HZSM-5 catalyst lifetime increased when 25 to 50 weight% water was co-fed with methanol at 698 K, but decreased below its maximum value when the fraction of water cofed was increased above 50 weight%.[30] The inhibitory effect of water co-feeds on coke formation has also been reported for light olefin conversion in the absence of methanol. Specifically, Luo *et al.* reported both decreasing conversions and lower amounts of coke deposited per gram of catalyst when water was cofed with C_2–C_4 olefins over HSAPO-34.[31] Overall, these studies point to the salient effects of water co-feeds on both induction periods as well as catalyst lifetimes in MTO conversion.

Competitive adsorption between water, oxygenates, and hydrocarbons has generally been offered as an explanation for the observed effects of water on catalyst lifetime and induction periods.[22,24,32] In addition to experimental studies, molecular dynamics simulations of water co-adsorption with methanol and propene onto Brønsted acid sites have also been used to support this proposal.[32] Haw and coworkers have proposed that water can alter the speciation of chain carriers constituting the hydrocarbon pool.[33] They noted that cofeeding 10 volume% water with methanol over HSAPO-34 at 673 K in pulse experiments led to an increase in average number of methyl groups per ring from 1.9 to 2.5, and concluded that the presence of water in the HSAPO-34 cavity increases the selectivity to methylbenzene molecules with a larger number of methyl groups per ring, leading to an increase in ethene selectivity. While competitive adsorption—widely used as a basis to rationalize the effect of water on MTO/MTH catalysis—represents a plausible explanation for longer induction periods resulting from an attenuation of reaction rates, it does not explain at a mechanistic level why co-feeding water leads to an increase in total turnovers. This study is motivated in part by the lack of a mechanistic proposal that explains both longer induction periods and higher total turnovers associated with water cofeeds. We provide computational and experimental evidence consistent with co-fed water effecting hydrolysis of hydroxymethyl intermediates formed in the transfer dehydrogenation of methanol, thereby resulting in a simultaneous attenuation of MTO chain initiation and termination rates. We present density functional theory calculations in section 3.1, transient experiments testing the reactivity of chloromethyl intermediates with water in section 3.2, and methanol-to-olefins catalysis data involving water co-feeds in section 3.3 to infer that Brønsted acid site-mediated hydrolysis of formaldehyde is an important factor contributing to observed effects of water co-feeds on methanol-to-olefins conversion.

2. Experimental

2.1 Catalyst synthesis and characterization

The detailed HSSZ-13 catalyst synthesis and characterization procedures for powder X-ray diffraction, N_2 physisorption, scanning electron microscopy, and ammonia temperature programmed desorption (TPD) were reported previously.[11] Briefly, the average crystallite size for the HSSZ-13 sample was approximately 450 nm, a micropore volume of 0.20 cm^3 g^{-1} was measured using N_2 physisorption, and the Brønsted acid site density measured using ammonia TPD was found to be 1.2 mmol H^+ g_{cat}^{-1}.

2.2 HSSZ-13 density functional theory calculations

The calculations reported herein were carried out using periodic plane-wave density functional theory (DFT) as implemented in the Vienna *ab initio* simulation program (VASP). The non-local exchange and correlation effects were treated using the Perdew–Burke–Erzenhof (PBE) exchange–correlation functional.[34] The core electrons were described using projector augmented wave (PAW) based pseudo-potentials.[35] The valence electrons were represented by a plane-wave basis set with an energy cutoff of 400 eV. Sampling of the Brillouin zone was performed at the Γ-point only due to the large size of the CHA unit cell and breaking of symmetry associated with Al substitution in the framework. The Grimme-type D3 corrections with Becke–Johnson (BJ) damping were applied to account for dispersive interactions.[36,37]

The self-consistent field calculations and geometric optimizations were converged to 10^{-6} eV and 0.05 eV $Å^{-1}$, respectively. More stringent self-consistent field criteria with energies $<10^{-6}$ eV or geometric optimization force criteria with forces <0.05 eV were determined to alter formaldehyde heat of adsorption in HSSZ-13 by less than 4 kJ mol^{-1}. Transition states were first identified *via* the climbing image nudged elastic band (CI-NEB) method[38,39] to a force tolerance of 0.3 eV $Å^{-1}$ and subsequently refined using the dimer method to within 0.05 eV $Å^{-1}$.[40] The dimer convergence criteria, similar to geometric optimizations, were determined to be invariant (<4 kJ mol^{-1} change in activation barrier) with lower force tolerance <0.05 eV $Å^{-1}$. Perturbation of the transition states to both sides of their associated mode and optimization back to the reactant and product confirms that the transition state is connected to both reactant and product states.

To obtain the free energies of reactants, products, and transition state structures resultant of the DFT calculations, harmonic frequency calculations (full Hessian vibrational analysis) were performed to determine zero-point vibrational energies (ZPVE), vibrational enthalpies (H_{vib}), and vibrational free energies (G_{vib}). Self-consistent field convergence at 10^{-8} eV and central difference method with atom displacement of 0.015 Å were used for the vibrational analysis. The immobile adsorbate method is applied in determination of reactant, product, and intermediate free energies and considered appropriate because of strong adsorptive binding of the oxygenated species (formaldehyde, methanediol, *etc.*) to the Brønsted acid site (section 3.1). The free energies are reported in sections S5–S7 of the ESI.†

The HSSZ-13 (CHA framework type) structure was constructed from the Accelrys Materials Studio structure library with unit cell $Si_{24}O_{48}$ and lattice parameters $a = b = c =$ 9.421 Å and $\alpha = \beta = \gamma = 94.200°$.[41] The CHA zeolite was modeled with a 2 × 2 supercell of 288 atoms where a single Al atom at the windows connecting the cages (Si/Al = 95) was substituted at the T1 site and balanced by a hydrogen atom to create a Brønsted acid site (Fig. 1).

2.3 Stoichiometric chloromethyl hydrolysis studies

The reactor setup used for chloromethyl hydrolysis experiments is described below (section 2.4). 125 mg of undiluted commercial HZSM-5 (Zeolyst CBV 2314; Si/Al = 11.5), with Brønsted acid site density of 12.9 ± 0.1 × 10^{-4} mol g^{-1} as assessed using DME titrations in a previous study,[42] was used in transient chloromethyl hydrolysis experiments. After the sample was treated under a flow of 1% O_2/He (0.42 cm^3 s^{-1}; Minneapolis Oxygen custom gas mixture UN1956) at 823 K for 28.8 ks, the temperature of the catalyst bed was decreased to 673 K under the same O_2–He atmosphere by ramping at 0.042 K s^{-1}, after which it was exposed to a flow of 0.67 cm^3 s^{-1} UHP helium. At the start of the transient experiment the flow was switched from helium to a 0.67 cm^3 s^{-1} UHP helium and 0.17 cm^3 s^{-1} argon stream into which dichloromethane (ACS reagent, 99.5%) was fed at a rate of 0.1 cm^3 h^{-1} while the effluent composition was monitored using a mass spectrometer. After 1.2 ks, which was sufficient for the dichloromethane signal to return to baseline levels, the catalyst was purged under a flow of 0.67 cm^3 s^{-1} helium for 3.6 ks followed by exposure to a 0.67 cm^3 s^{-1} UHP helium and 0.17 cm^3 s^{-1} argon stream injected with deionized water at 0.1 cm^3 h^{-1}. We note that the only products observed above baseline levels when the zeolite was exposed to dichloromethane were hydrochloric acid, dichloromethane, and water; similarly, the only product detected when the bed containing chloromethyl intermediates was exposed to water was hydrochloric acid (section S9, ESI†). After the HCl signal on the mass spectrometer returned to baseline levels the catalyst was regenerated under 1% O_2–He for replicate runs. The total amount of reactant consumed/product generated was calculated by integrating the corresponding signal with reference to the baseline using helium as the internal standard.

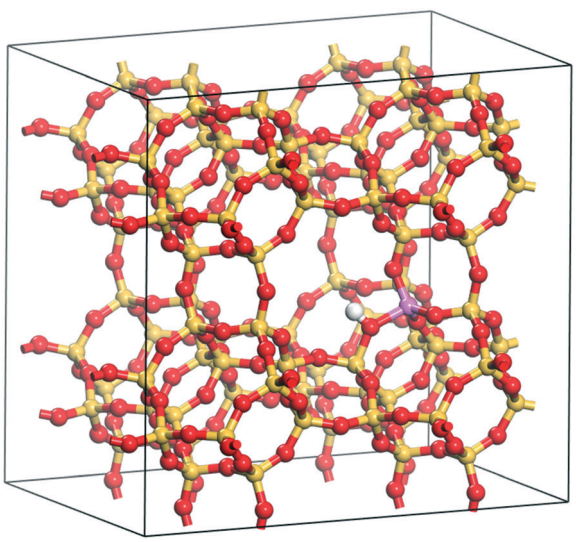

Fig. 1 2 × 2 super cell of zeolite CHA with Al substituted at the T1 position to form the associated Brønsted acid site. Atom colors: Al (purple), Si (yellow), O (red), and H (white).

2.4 Methanol-to-olefins catalysis

Methanol-to-olefins conversion over HSSZ-13 was assessed using a quartz tube (4 mm diameter) placed in a custom-built single-zone copper furnace, the temperature of which was controlled using two 250 W Omega Engineering cartridge heaters (CSH-202250). The temperature was measured using a K-type thermocouple inserted axially and penetrating the top of the catalyst bed. The sample was treated in a 1% O_2/He mixture (0.42 cm^3 s^{-1}; Minneapolis Oxygen custom gas mixture UN1956) by ramping to 823 K at 0.018 K s^{-1} to remove the organic template used in zeolite synthesis. After holding at 823 K for 28.8 ks, the temperature of the catalyst bed was decreased to reaction temperature (623–673 K) under the same O_2–He atmosphere by ramping at 0.042 K s^{-1}, after which it was exposed to a flow of 0.83 cm^3 s^{-1} He (Minneapolis Oxygen, 99.997%) for 3.6 ks. Using a syringe pump, solutions containing appropriate weight ratios of methanol (Aldrich CHROMASOLV HPLC grade (>99.9% purity)) and deionized water were injected at the desired flow rate into heated gas lines (>383 K) carrying helium and argon (internal standard). Reaction products were quantified using an Agilent 7890A GC system with a HP-PLOT Q column connected to a thermal conductivity detector (He as reference gas) and an HP-1 column connected to a flame ionization detector. A VICI Valco 16-port multi-position sample valve was used in conjunction with a 10-port two-position sample valve on the GC to measure data points at time intervals as small as 45 seconds. The results reported are based on data acquired at sub-complete methanol conversion; specifically, the highest conversion data point in the experiments

reported in this study was 61.4%. The turnover number (TON) was calculated as the time-on-stream integral of the sum of hydrocarbon site time yields weighted by carbon number. Initiation rates are calculated as the derivative of the total hydrocarbon site time yield with respect to time-on-stream during the induction period (period associated with increasing hydrocarbon site time yield as a function of time-on-stream) and termination rates are calculated as the negative derivative of total hydrocarbon site time yield with respect to time-on-stream during the deactivation period (period associated with decreasing hydrocarbon site time yield as a function of time-on-stream) with an illustrative example provided in the ESI† (section S11).

3. Results

3.1 HSSZ-13 density functional theory calculations

DFT calculations for H_2O addition to formaldehyde were carried out using the HSSZ-13 zeolite model described in section 2.2 to examine the following elementary steps (fractional coordinates provided in section S1, optimized structures in section S3, energies in section S5, ESI†):

$$HCHO(gas) + H^+\text{-Zeolite} \rightleftharpoons HCHO\text{–}H^+\text{-Zeolite}$$
(formaldehyde adsorption)

$$HCHO\text{–}H^+\text{-Zeolite} \rightleftharpoons H_2C^+OH\text{-Zeolite}$$
(formaldehyde protonation)

$$H_2O(gas) + H_2C^+OH\text{-Zeolite} \rightleftharpoons H_2O\text{–}H_2C^+OH\text{-Zeolite}$$
(water adsorption)

$$H_2O\text{–}H_2C^+OH\text{-Zeolite} \rightleftharpoons H_2C(OH)_2\text{–}H^+\text{-Zeolite}$$
(hydroxymethyl hydrolysis)

$$H_2C(OH)_2\text{–}H^+\text{-Zeolite} \rightleftharpoons H_2C(OH)_2(gas) + H^+\text{-Zeolite}$$
(methanediol desorption)

The electronic energy profile for formaldehyde hydrolysis is provided in Fig. 2. Formaldehyde was calculated to have a heat of adsorption of −83 kJ mol^{-1} in HSSZ-13. Given the lack of reported experimental values for the heat of adsorption of formaldehyde, we tested the reliability of our calculations using acetone as a surrogate for formaldehyde. Our calculated heat of adsorption of acetone in HZSM-5 of −139 kJ mol^{-1} compares well with published values of −130 kJ mol^{-1} measured using microcalorimetry[43] and −139 kJ mol^{-1} resulting from *ab initio* calculations using a large zeolite cluster model and embedding methods.[44] The heat of adsorption of acetone is stronger than that of formaldehyde as the oxygen of a ketone is more basic than that of an aldehyde with reported gas phase proton affinities of 812 and 713 kJ mol^{-1} for acetone and formaldehyde, respectively.[45] Once adsorbed into the zeolite cavity, formaldehyde undergoes protonation at a Brønsted acid site to form a hydroxymethyl intermediate (H_2C^+OH) with an intrinsic barrier of 19 kJ mol^{-1}. Water is physisorbed into the zeolite pore with a heat of adsorption of 43 kJ mol^{-1} which is comparable with experimentally measured values of negative 43–51 kJ mol^{-1} on HZSM-5.[46,47]

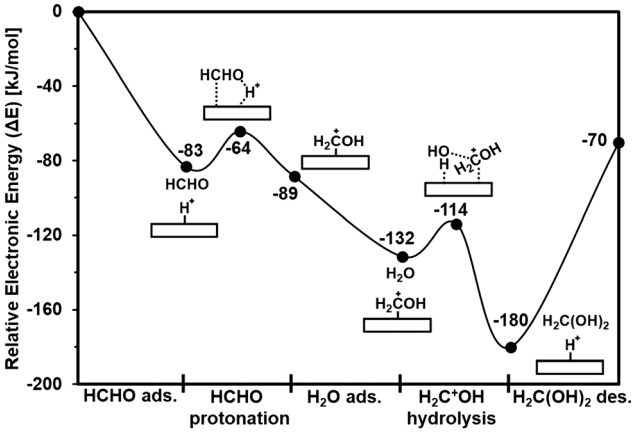

Fig. 2 Electronic energy profile for the full turnover cycle for HCHO + $H_2O \rightarrow H_2C(OH)_2$ over HSSZ-13.

Further hydrolysis of the hydroxymethyl intermediate by reaction with an adsorbed water molecule occurs with an intrinsic barrier of 18 kJ mol^{-1}. The framework oxygen atoms at the substituted Al active site stabilize both the proton from water and the OH of the planar hydroxymethyl carbenium ion that forms in the transition state where the C–O bond elongates from 1.587 Å in the adsorbed hydroxymethyl reactant state to 2.299 Å in the transition state. The planar hydroxymethyl carbenium ion interacts closely with the incoming water molecule with a C(hydroxymethyl)–O(water) distance of 3.132 Å in the transition state (Fig. 3). The intrinsic activation barrier for C–O bond formation in the hydroxymethyl hydrolysis step between the hydroxymethyl intermediate and water is 18 kJ mol^{-1}. In comparison, prior literature that examined methyl hydrolysis over HZSM-5 reported intrinsic activation barriers for C–O bond formation between the methyl intermediate and water of +112 kJ mol^{-1} (ref. 48) and +81.8 kJ mol^{-1}.[49] Thus, the hydroxymethyl intermediate appears to undergo hydrolysis more readily compared to methyl intermediates. The hydroxymethyl cation (CH_2OH^+) that forms in the transition state is much more stable than the methyl cation (CH_3^+) as it can more readily delocalize the positive charge. In addition, the transition state for the hydroxymethyl cation water complex (CH_2–OH^+–H_2O) is stabilized *via* direct interaction with the zeolite as both the water and hydroxymethyl protons interact with the framework lattice oxygen (with O–H distances of 1.904 Å and 1.297 Å) to form a cyclic transition state as shown in Fig. 3. The low barrier for hydrolysis appears to arise due to these strong interactions forming a "cyclic" transition state consisting of alternating partially positive and negative species. The DFT calculations show an overall electronic energy change of −70 kJ mol^{-1} suggesting formaldehyde hydrolysis is exothermic. These DFT calculations point to the plausibility of hydroxymethyl hydrolysis over HSSZ-13 Brønsted acid sites. We also carried out calculations for chloromethyl hydrolysis, used as

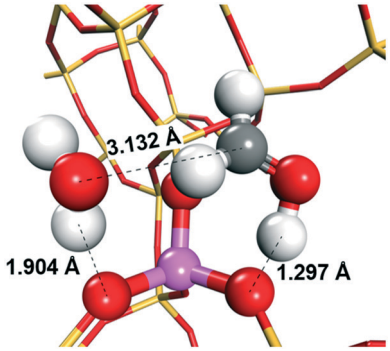

Fig. 3 DFT calculated transition state for H_2C^+OH hydrolysis where dotted lines indicate close interaction between atoms, either electrostatic or van der Waals. Atom colors: Al (purple), Si (yellow), O (red), C (gray), and H (white).

a surrogate for hydroxymethyl hydrolysis in our transient experimental studies. Fractional coordinates (section S2), optimized structures (section S4), energies (section S6), and electronic energy profiles (section S10) are reported as ESI.† These calculations show an overall electronic energy change of −6 kJ mol^{-1}. Unlike hydroxymethyl hydrolysis which occurs *via* a stabilized "cyclic" transition state, electrostatic repulsion between Cl of chloromethyl and O of zeolite (Fig. S4f†) causes higher barriers for its hydrolysis compared to hydroxymethyl. Further, similar free energies of activation for the carbon–oxygen bond formation step over HSSZ-13 (131 kJ mol^{-1}) and HZSM-5 (137 kJ mol^{-1}) indicate that conclusions relating to the plausibility of hydrolysis are independent of the identity of the framework (section S6 and S7, ESI†). Overall, these electronic energy and free energy values are consistent with the occurrence of chloromethyl hydrolysis over HZSM-5 observed in our study as well as the plausibility of occurrence of hydroxymethyl hydrolysis over HSSZ-13 used in the interpretation of trends in MTO data as a function of water co-feed partial pressure (section 3.3).

3.2 Chloromethyl hydrolysis experiments

Direct experimental verification of hydrolysis of hydroxymethyl intermediates using transient kinetic experiments is challenging as aqueous solutions of formaldehyde typically contain significant amounts of methanediol.[50] Additionally, equilibrium constants tending towards formaldehyde with increasing temperature[51,52] suggest that a significant fraction of the methanediol formed could decompose to formaldehyde and water in the mass spectrometer. As an alternative, we investigated the formation and hydrolysis of intermediates formed in dicholoromethane reactions over HZSM-5 (Si/Al ratio 11.5) at 673 K. Our goal in pursuing these experiments was to demonstrate the plausibility of forming a hydroxymethyl intermediate (CH_2OH^*) by depositing CH_2Cl^* in a stoichiometric reaction ($CH_2Cl_2 + H^* \rightarrow CH_2Cl^* + HCl$) and to demonstrate feasibility of hydrolyzing a hydroxymethyl intermediate to form methanediol ($CH_2OH^* + H_2O \rightarrow CH_2(OH)_2 + H^*$) by stoichiometrically hydrolyzing the CH_2Cl^* intermediate ($CH_2Cl^* + H_2O \rightarrow OH(CH_2)Cl + H^*$). We make no attempt to compare rates of the elementary steps involved in these events since these cannot be inferred from the stoichiometric experiments we have pursued. Replacing the hydroxyl group with a chlorine atom renders the chloromethyl intermediate persistent; also, chloromethanol formed on exposure to water decomposes to formaldehyde and hydrochloric acid (Scheme 1)—products distinct from the reactants, both of which can be detected using a mass spectrometer. HZSM-5 was chosen for these transient experiments owing to its larger pore opening (5.5 Å) compared to HSSZ-13 (3.8 Å),[53] thereby reducing experimental artifacts resulting from diffusion limitations. Dichloromethane consumed and hydrochloric acid produced upon exposing HZSM-5 to dichloromethane (step 1) and, water consumed and hydrochloric acid formed upon exposure to water (step 2) correspond, within error, to the number of Brønsted acid sites present in the HZSM-5 bed (Fig. 4). This is consistent with both the persistent nature of chloromethyl intermediates and the occurrence of chloromethyl hydrolysis at 673 K. Based on the one-to-one correspondence between HCl produced and the number of Brønsted acid sites present in these experiments, we posit that this chemistry can occur at MTO-relevant temperatures, independent of the zeolite framework under consideration.

3.3 Methanol-to-olefins catalysis

The methanol : DME ratio influences MTO/MTH catalyst lifetime, with HZSM-5 carbon conversion capacities at 623 K tracking with effluent DME : methanol ratios for DME, DME–water, and methanol feeds.[14] One of the ways water co-feeds can influence MTO performance is by increasing effluent methanol : DME ratios and average methanol pressures. More specifically, a monotonic increase in methanol : DME ratio with water co-feed pressures would suggest that water co-feeds accelerate MTO chain initiation and termination on

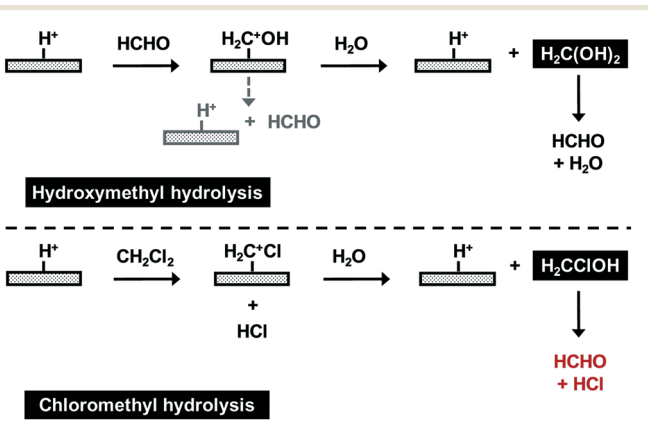

Scheme 1 Reaction steps involved in the formation and hydrolysis of hydroxymethyl (top) and chloromethyl (bottom) intermediates on zeolitic Brønsted acid sites.

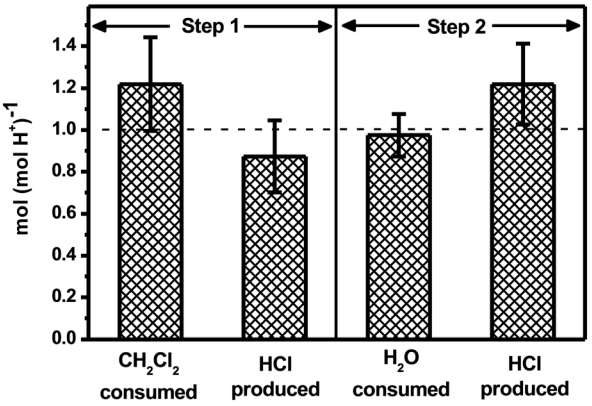

Fig. 4 Moles of reactant consumed/product formed in transient experiments involving chloromethylation (step 1: 673 K, 3.7 kPa CH_2Cl_2, 18.7 mol CH_2Cl_2 (mol H^+)$^{-1}$ h^{-1}) and chloromethyl hydrolysis (step 2; 673 K, 12 kPa H_2O, 67 mol H_2O (mol H^+)$^{-1}$ h^{-1}) over 125 mg HZSM-5 (Si : Al = 11.7).

account of increasing average methanol pressures resulting from higher net rates of DME hydrolysis. Methanol–DME approach to equilibrium values (eqn (1)) below 0.01 at all turnover numbers and water co-feed pressures (Fig. 5, top), and resulting effluent methanol : DME ratios that are roughly invariant in water pressure (Fig. 5, bottom) suggest that the effect of water on initiation and termination rates under the experimental conditions used in this study likely cannot be rationalized on the basis of increased occurrence of DME hydrolysis.

$$\eta_{\mathrm{MeOH-DME}} = \frac{\left[P_{\mathrm{DME}}\right]\left[P_{\mathrm{H_2O}}\right]}{\left[P_{\mathrm{MeOH}}\right]^2 K_{\mathrm{MeOH-DME}}} \quad (1)$$

$\eta_{\mathrm{MeOH-DME}}$: methanol–DME approach to equilibrium; $[P_i]$ partial pressure (in atm) of species i at the reactor outlet; $K_{\mathrm{MeOH-DME}}$: equilibrium constant for methanol dehydration to DME at a particular temperature.

The acceleration/deceleration of product formation during autocatalysis, calculated as the derivative of hydrocarbon site time yield with respect to time-on-stream during the induction and deactivation periods respectively (eqn (2) and (3)), can be considered as representative of the rates of chain initiation and termination in MTO catalysis.[19] The critical role of formaldehyde in initiating and terminating MTO chain propagation cycles (*vide supra*) implies that scavenging of formaldehyde by water—suggested plausible by both density functional theory calculations and transient stoichiometric experiments—should lead to a decrease in initiation and termination rates (reflected in a decrease in acceleration and deceleration of product formation respectively), and a simultaneous increase in total turnovers (Scheme 2). Co-feeding 0–58 kPa water at 673 K leads to monotonically decreasing initiation rates from 11.6×10^{-4} to 4.9×10^{-4} mol C (mol H^+)$^{-1}$ h^{-2},

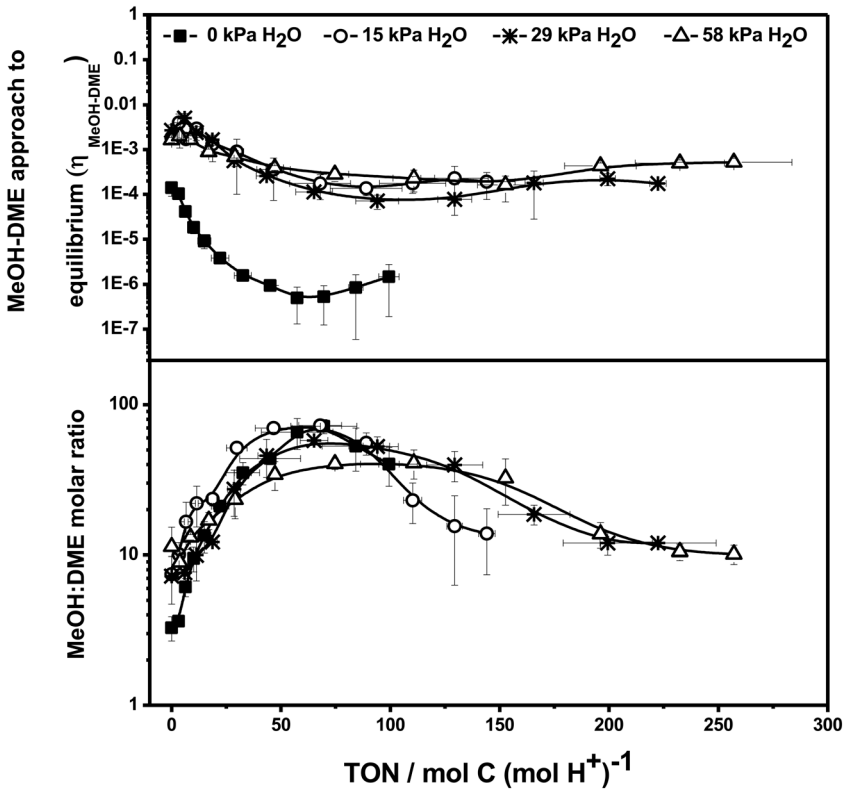

Fig. 5 Methanol–DME approach to equilibrium (top) and reactor effluent methanol : DME molar ratio (bottom); 673 K, 5.8 kPa MeOH, 0–58 kPa H_2O, 35.34 g_{MeOH} g_{cat}^{-1} h^{-1}, 10 mg HSSZ-13, 100 mg quartz sand.

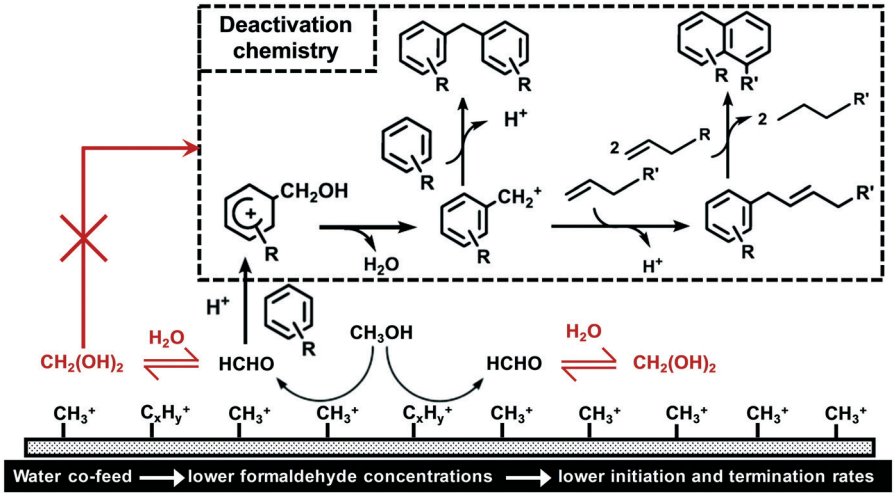

Scheme 2 Pictorial depiction of the mechanistic basis for the effect of water co-feeds on chain initiation and termination rates: formaldehyde, formed in the transfer dehydrogenation of methanol with alkoxides, reacts with water to form methanediol. Unlike formaldehyde, methanediol does not participate in chain initiation and termination events.

monotonically decreasing termination rates from 10.7×10^{-6} to 5.4×10^{-6} mol C (mol H^+)$^{-1}$ h^{-2}, and a concurrent monotonic increase in turnover capacity from 88 to 280 mol C (mol H^+)$^{-1}$ (Fig. 6), consistent with higher partial pressures of water leading to a larger fraction of the formaldehyde formed being hydrolyzed to methanediol, thereby attenuating the relative degree of formaldehyde-induced MTO chain initiation and termination. We note that small changes in formaldehyde concentration (on the order of a few Pa in pressure) can result in discernible effects on chain initiation/termination rates and total turnovers, as demonstrated by the observation that a 10 Pa formaldehyde co-feed (methanol : formaldehyde molar ratio = 2300) can result in a reduction in total turnovers of approximately 15% despite the fact that only a fraction of the co-fed formaldehyde may have diffused through the 3.8 Å pore opening of HSSZ-13.[11] In another set of experiments, co-reacting formaldehyde (11 Pa or 3 carbon%) with propylene (0.1 kPa) over HZSM-5 at 623 K was shown to result in a 5.5-fold increase in aromatics selectivity, again suggesting that small amounts of formaldehyde may be sufficient to significantly alter chain initiation rates.[20] More specifically, Liu *et al.* reported mass spectrometry data pointing to a formaldehyde partial pressure of 10.8 Pa at 0.24% methanol conversion over HZSM-5 at 748 K.[16] Although reliable quantitative estimates of the concentration of formaldehyde present are not accessible in the experiments reported here, the trends shown in Fig. 6 are nevertheless consistent with our mechanistic hypothesis.

$$\text{Initiation rate} = +\frac{\partial(\text{total hydrocarbon site time yield})}{\partial t} \quad (2)$$

$$\text{Termination rate} = -\frac{\partial(\text{total hydrocarbon site time yield})}{\partial t} \quad (3)$$

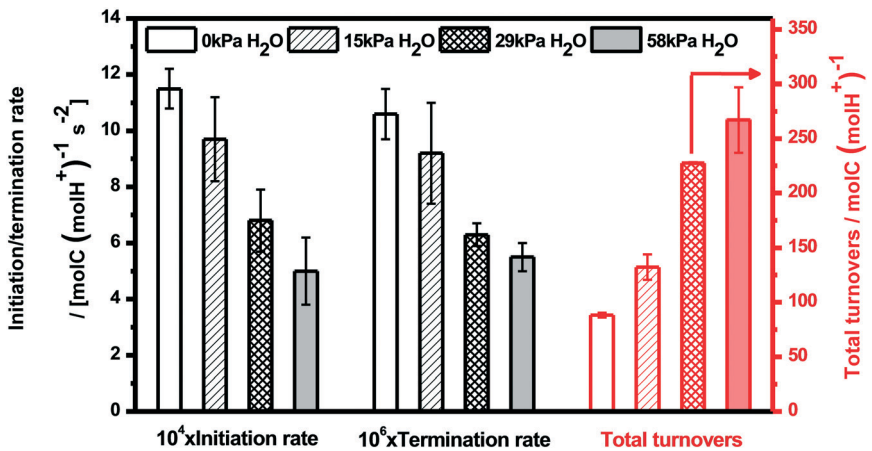

Fig. 6 Initiation rates, termination rates, and total turnover capacities as a function of water co-feed pressure: 673 K, 5.8 kPa MeOH, 0–58 kPa H_2O, 35.34 g_{MeOH} g_{cat}^{-1} h^{-1}, 10 mg HSSZ-13, 100 mg quartz sand.

In addition, trends as a function of temperature in the presence of water co-feeds can be rationalized on the basis of equilibrium being achieved between formaldehyde, water, and methanediol under the experimental conditions used in this study. The highly exothermic nature of formaldehyde hydrolysis (−70 kJ mol^{-1} in Fig. 2) suggests that equilibrium constants for the reaction decrease with increasing temperature, a trend that has been reported in theoretical studies in the literature.[50,51] Such an inverse correlation between hydrolysis equilibrium constants and temperature dictates that under conditions where formaldehyde is equilibrated with methanediol, co-feeding water at the same partial pressure should lead to a larger fraction of the formaldehyde formed at that temperature being present as methanediol at lower temperatures relative to that at higher temperatures. Consistent with this expectation, initiation rates, termination rates, and turnover capacities normalized by their corresponding values in the absence of a water co-feed at the same temperature show a larger deviation from unity at lower temperatures (Fig. 7), implying that the presence of an equivalent pressure of water has a larger impact on initiation and termination rates at lower temperatures relative to higher ones. These data demonstrate the importance of accounting for formaldehyde hydrolysis chemistry when assessing the mechanistic role of water in methanol-to-olefins conversion processes.

Slower initiation rates with increasing water partial pressure in the co-feed are consistent with the reported increase in the duration of the induction period on co-feeding water with methanol over HSAPO-34[22,32] and HMOR.[24] The observed increase in total turnovers is consistent with the reported increase in catalyst lifetime over HSAPO-34,[22,23] HMOR,[24] and HZSM-58,[25] as well as the reported decrease in amount of carbon deposited per gram catalyst at equivalent times-on-stream over HSAPO-34,[26,27] HSAPO-18,[28] and HZSM-5.[29] The effect of co-feeding water on induction periods has typically been attributed to the competitive adsorption of water with methanol or olefins onto Brønsted acid sites.[22,23] We note that while competitive adsorption can explain longer induction periods resulting from the inhibiting effect of water on the reactivity of molecules like methanol and propene, a clear mechanistic explanation as to why water increases the number of total turnovers based on the idea of competitive adsorption has not been offered so far. The aforementioned reports aimed at understanding the mechanistic basis for water-induced mitigation of catalyst deactivation, but a discussion of the role of water in context of reactions responsible for chain initiation and termination has been lacking, partly because mechanistic understanding of catalyst deactivation did not exist when most of these studies were conducted. For example, Marchi and Froment[22] and Wu and Anthony[23] attributed longer HSAPO-34 catalyst lifetimes to preferential adsorption of water on stronger acid sites presumed to be responsible for coke formation. Weckhuysen and coworkers[32] used molecular dynamics simulations to show that water inhibits the reactivity of methanol and propene over HSAPO-34 Brønsted acid sites. Using UV-vis microspectroscopy and *in situ* confocal experiments they demonstrated that co-feeding water leads to more uniform deposition of coke throughout the crystals, unlike in the absence of water co-feeds where preferential deposition of coke on the outer rim of the crystal was detected. These reports do not assess the effect of water in the context of the recent

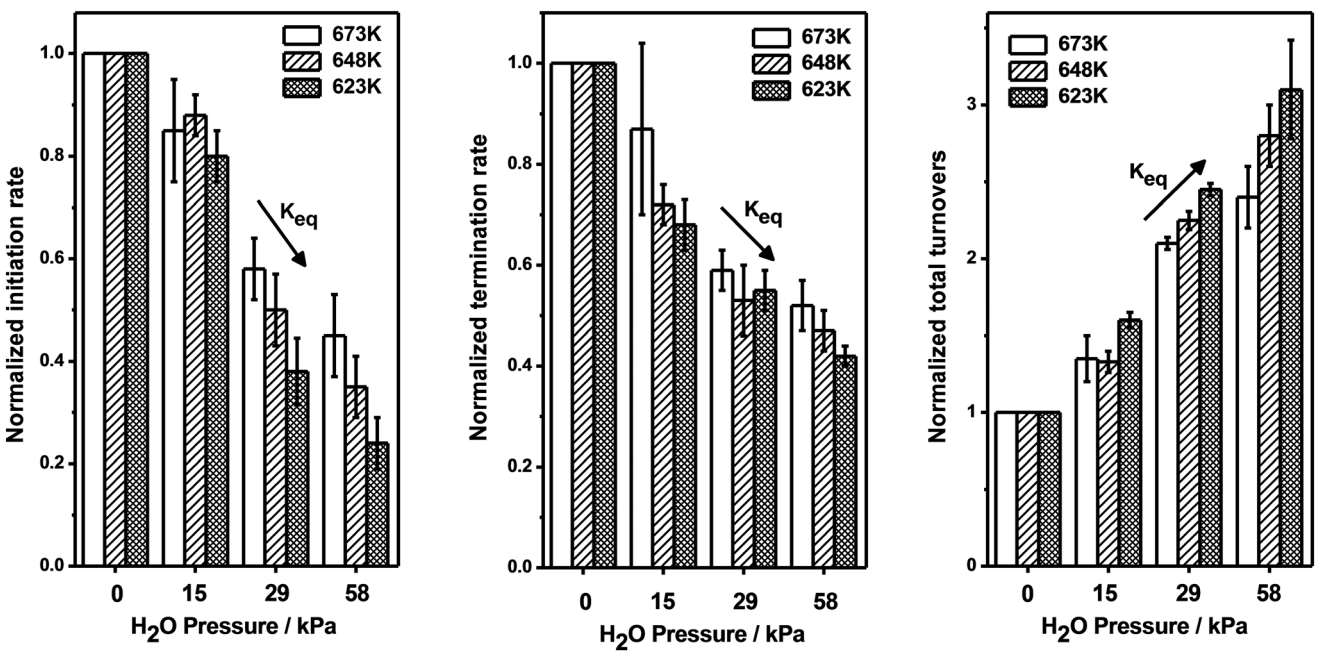

Fig. 7 Normalized initiation rates (left), termination rates (center), and total turnovers (right) as a function of water co-feed pressure at three temperatures (623, 648, and 673 K); 5.8 kPa MeOH, 0–58 kPa H_2O, 35.34 g_{MeOH} g_{cat}^{-1} h^{-1}, 10 mg HSSZ-13, 100 mg quartz sand; initiation rates, termination rates, and turnover capacities are normalized by corresponding values in the absence of water co-feeds at the same temperature.

advances in our understanding of the identity of intermediates and reaction steps involved in formaldehyde-mediated chain initiation and termination.[11–15,17–20] The plausibility of hydroxymethyl hydrolysis, combined with the rationalization of the effect of water cofeeds on both chain initiation and termination rates presented here, rationalizes the effect of water cofeeds reported in the literature with reaction pathways mediating chain initiation and termination recently elucidated in the literature. Crucially, the scavenging of formaldehyde by co-fed water explains both longer induction periods as well as longer catalyst lifetimes and provides a mechanistic explanation for the favorable effect of water on catalyst lifetime that has so far been lacking in the literature.

Despite the conspicuous effect of water on initiation and termination rates, water co-feeds appear not to have a discernible effect on cumulative ethene, propene, and C_2–C_4 paraffin yields when plotted as a function of turnover number—a rigorous descriptor of reaction progress (Fig. 8).[11,19,54,55] Cumulative product yields as a function of turnover number that are invariant with water co-feed pressure suggest that water can inhibit chain initiation and termination events without necessarily altering the speciation of active chain carriers constituting the hydrocarbon pool. This interpretation of cumulative product selectivity as a function of turnover number contrasts with erroneous interpretations of selectivity data at dissimilar methanol conversions/turnover numbers previously used as a basis for proposing that water co-feeds increase light olefin (ethene and propene)[22,23] and C_3^+ olefin[24] selectivities. These results imply that co-feeding water offers a strategy for increasing total turnovers on CHA materials without adversely affecting cumulative light-olefin selectivities.

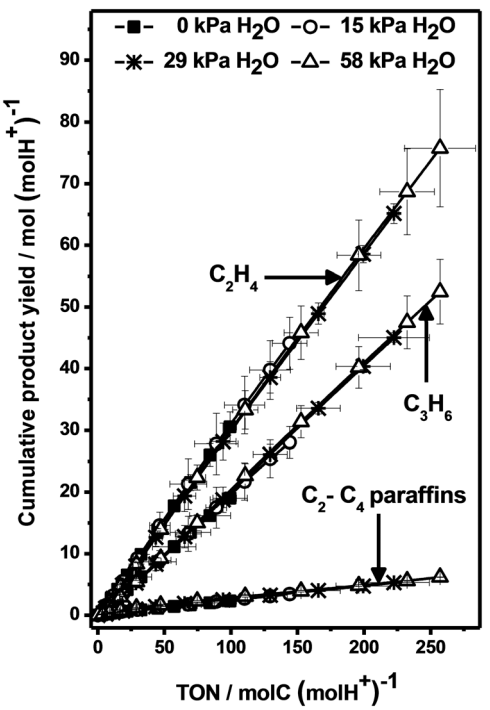

Fig. 8 Cumulative ethene, propene, and C_2–C_4 paraffin yields as a function of turnover number; 673 K, 5.8 kPa MeOH, 0–58 kPa H_2O, 35.34 g_{MeOH} g_{cat}^{-1} h^{-1}, 10 mg HSSZ-13, 100 mg quartz sand.

4. Conclusions

Co-feeding water with methanol over HSSZ-13 at 623–673 K results in initiation and termination MTO rates that monotonically decrease, and turnover capacities that monotonically increase with water co-feed partial pressure. Density functional theory calculations support the plausibility of hydroxymethyl hydrolysis and transient chloromethyl hydrolysis experiments show that surface intermediates similar to hydroxymethyl species can be formed and hydrolyzed at MTO-relevant temperatures (623–673 K). Normalized initiation/termination rates and total turnovers that follow expected trends as a function of reaction temperature assuming equilibrium is achieved between formaldehyde and methanediol emphasize the critical role of formaldehyde hydrolysis chemistry on chain initiation and termination steps under the experimental conditions used in this study. This enhancement in turnover capacity is achieved without any significant alteration in the speciation of hydrocarbon pool chain carriers, resulting in cumulative light-olefin selectivities that are invariant in water co-feed pressure. These results point to the efficacy of co-feeding water as a strategy for improving HSSZ-13 catalyst lifetime while also highlighting the saliency of formaldehyde hydrolysis chemistry on MTO chain initiation, propagation, and termination events.

Conflicts of interest

There are no conflicts of interest to declare.

Acknowledgements

We gratefully acknowledge financial support from Dow through the University Partnership Initiative, the National Science Foundation (CBET 1701534), and computational resources from the Minnesota Supercomputing Institute. We thank Dr. Andrew Hwang, Mr. Sukaran Arora, and Mr. Brandon Foley for helpful technical discussions.

References

1 M. A. Rouhi, *Chem. Eng. News*, 2015, **31**, 30.
2 N. Y. Chen and W. J. Reagan, *J. Catal.*, 1979, **59**, 123–129.
3 R. L. Espinoza, *Appl. Catal.*, 1986, **26**, 203–209.
4 S. Ilias and A. Bhan, *ACS Catal.*, 2013, **3**, 18–31.
5 S. Ilias and A. Bhan, *J. Catal.*, 2012, **290**, 186–192.
6 I. M. Dahl and S. Kolboe, *Catal. Lett.*, 1993, **20**, 329–336.
7 M. Bjørgen, F. Joensen, K. P. Lillerud, U. Olsbye and S. Svelle, *Catal. Today*, 2009, **142**, 90–97.
8 S. Teketel, U. Olsbye, K. P. Lillerud, P. Beato and S. Svelle, *Microporous Mesoporous Mater.*, 2010, **136**, 33–41.
9 R. Khare, D. Millar and A. Bhan, *J. Catal.*, 2015, **321**, 23–31.

10 S. Svelle, F. Joensen, J. Nerlov, U. Olsbye, K. P. Lillerud, S. Kolboe and M. Bjørgen, *J. Am. Chem. Soc.*, 2006, **128**, 14770–14771.
11 A. Hwang, M. Kumar, J. D. Rimer and A. Bhan, *J. Catal.*, 2017, **346**, 154–160.
12 S. Müller, Y. Liu, M. Vishnuvarthan, X. Sun, A. C. Van Veen, G. L. Haller, M. Sanchez-Sanchez and J. A. Lercher, *J. Catal.*, 2015, **325**, 48–59.
13 Y. Li, M. Zhang, D. Wang, F. Wei and Y. Wang, *J. Catal.*, 2014, **311**, 281–287.
14 J. S. Martinez-Espin, M. Mortén, T. V. W. Janssens, S. Svelle, P. Beato and U. Olsbye, *Catal. Sci. Technol.*, 2017, **7**, 2700–2716.
15 J. S. Martínez-Espín, K. De Wispelaere, T. V. W. Janssens, S. Svelle, K. P. Lillerud, P. Beato, V. Van Speybroeck and U. Olsbye, *ACS Catal.*, 2017, **7**, 5773–5780.
16 Y. Liu, F. M. Kirchberger, S. Müller, M. Eder, M. Tonigold, M. Sanchez-Sanchez and J. A. Lercher, *Nat. Commun.*, 2019, **10**, 1–9.
17 X. Sun, S. Mueller, Y. Liu, H. Shi, G. L. Haller, M. Sanchez-Sanchez, A. C. Van Veen and J. A. Lercher, *J. Catal.*, 2014, **317**, 185–197.
18 S. Müller, Y. Liu, F. M. Kirchberger, M. Tonigold, M. Sanchez-Sanchez and J. A. Lercher, *J. Am. Chem. Soc.*, 2016, **138**, 15994–16003.
19 A. Hwang and A. Bhan, *ACS Catal.*, 2017, **7**, 4417–4422.
20 S. S. Arora and A. Bhan, *J. Catal.*, 2017, **356**, 300–306.
21 B. E. Langner, *Appl. Catal.*, 1982, **2**, 289–302.
22 A. J. Marchi and G. F. Froment, *Appl. Catal.*, 1991, **71**, 139–152.
23 X. Wu and R. G. Anthony, *Appl. Catal., A*, 2001, **218**, 241–250.
24 A. J. Marchi and G. F. Froment, *Appl. Catal., A*, 1993, **94**, 91–106.
25 Y. Kumita, J. Gascon, E. Stavitski, J. A. Moulijn and F. Kapteijn, *Appl. Catal., A*, 2011, **391**, 234–243.
26 A. T. Aguayo, A. G. Gayubo, A. Atutxa, M. Olazar and J. Bilbao, *J. Chem. Technol. Biotechnol.*, 1999, **74**, 1082–1088.
27 A. G. Gayubo, A. T. Aguayo, A. E. Sánchez Del Campo, A. M. Tarrío and J. Bilbao, *Ind. Eng. Chem. Res.*, 2000, **39**, 292–300.
28 A. G. Gayubo, A. T. Aguayo, A. Alonso, A. Atutxa and J. Bilbao, *Catal. Today*, 2005, **106**, 112–117.
29 P. Pérez-Uriarte, A. Ateka, A. T. Aguayo, A. G. Gayubo and J. Bilbao, *Chem. Eng. J.*, 2016, **302**, 801–810.
30 M. Ghavipour, R. M. Behbahani, G. R. Moradi and A. Soleimanimehr, *Fuel*, 2013, **113**, 310–317.
31 M. Luo, Y. Fu, B. Hu, D. Wang, B. Wang and G. Mao, *Appl. Catal., A*, 2019, **570**, 209–217.
32 K. De Wispelaere, C. S. Wondergem, B. Ensing, K. Hemelsoet, E. J. Meijer, B. M. Weckhuysen, V. Van Speybroeck and J. Ruiz-Martínez, *ACS Catal.*, 2016, **6**, 1991–2002.
33 W. Song, H. Fu and J. F. Haw, *J. Am. Chem. Soc.*, 2001, **123**, 4749–4754.
34 J. P. Perdew, K. Burke and M. Ernzerhof, *Phys. Rev. Lett.*, 1996, **77**, 3865–3868.
35 P. E. Blöchl, *Phys. Rev. B: Condens. Matter Mater. Phys.*, 1994, **50**, 17953–17979.
36 S. Grimme, J. Antony, S. Ehrlich and H. Krieg, *J. Chem. Phys.*, 2010, **132**, 154104.
37 S. Grimme, S. Ehrlich and L. Goerigk, *J. Comput. Chem.*, 2011, **32**, 1456–1465.
38 G. Henkelman and H. Jónsson, *J. Chem. Phys.*, 2000, **113**, 9978–9985.
39 G. Henkelman, B. P. Uberuaga and H. Jónsson, *J. Chem. Phys.*, 2000, **113**, 9901–9904.
40 G. Henkelman and H. Jónsson, *J. Chem. Phys.*, 1999, **111**, 7010–7022.
41 Materials Studio (Accelrys Inc.), Database of Structures.
42 J. Bedard, D. Y. Hong and A. Bhan, *J. Catal.*, 2013, **306**, 58–67.
43 J. Šepa, C. Lee, R. J. Gorte, D. White, E. Kassab, E. M. Evleth, H. Jessri and M. Allavena, *J. Phys. Chem.*, 1996, **100**, 18515–18523.
44 B. Boekfa, J. Sirijareansre, P. Panta and J. Limtrakul, *Stud. Surf. Sci. Catal.*, 2004, **154**, 1582–1588.
45 E. P. L. Hunter and S. G. Lias, *J. Phys. Chem. Ref. Data*, 1998, **27**, 413–656.
46 K. Zhang, R. P. Lively, J. D. Noel, M. E. Dose, B. A. McCool, R. R. Chance and W. J. Koros, *Langmuir*, 2012, **28**, 8664–8673.
47 A. Ison and R. J. Gorte, *J. Catal.*, 1984, **89**, 150–158.
48 J. Meeprasert, S. Jungsuttiwong, T. N. Truong and S. Namuangruk, *J. Mol. Graphics Modell.*, 2013, **43**, 31–40.
49 S. Namuangruk, J. Meeprasert, P. Khemthong and K. Faungnawakij, *J. Phys. Chem. C*, 2011, **115**, 11649–11656.
50 D. R. Kent, S. L. Widicus, G. A. Blake and W. A. Goddard, *J. Chem. Phys.*, 2003, **119**, 5117–5120.
51 M. Rodler, *Chem. Phys.*, 1986, **105**, 345–353.
52 E. L. Piret and M. W. Hall, *Ind. Eng. Chem.*, 1940, **32**, 1016–1018.
53 F. Gao, E. D. Walter, E. M. Karp, J. Luo, R. G. Tonkyn, J. H. Kwak, J. Szanyi and C. H. F. Peden, *J. Catal.*, 2013, **300**, 20–29.
54 A. Hwang, D. Prieto-Centurion and A. Bhan, *J. Catal.*, 2016, **337**, 52–56.
55 P. Bollini and A. Bhan, *ChemPhysChem*, 2018, **19**, 1–6.